Characterization of Surface-Modified Hollow Fiber Polyethersulfone Membranes Prepared at Different Air Gaps

K. C. Khulbe,[1] C. Y. Feng,[1] T. Matsuura,[1] D. C. Mosqueada-Jimenaez,[2] M. Rafat,[1] D. Kingston,[3] R. M. Narbaitz,[2] M. Khayet[4]

[1]*Department of Chemical Engineering, IMRI, University of Ottawa, Ottawa, Ontario, Canada K1N 6N5*
[2]*Department of Civil Engineering, University of Ottawa, Ottawa, Ontario, Canada K1N 6N5*
[3]*Nanostructure Material Research Group, National Research Council of Canada, Ottawa, Ontario, Canada K1A 0R6*
[4]*Department of Applied Physics, University Complutense of Madrid, Madrid, Spain*

Received 5 January 2006; accepted 9 May 2006
DOI 10.1002/app.24853
Published online in Wiley InterScience (www.interscience.wiley.com).

ABSTRACT: Hollow fibers were spun from a solution of surface-modifying macromolecule blended polyethersulfone in dimethyl acetamide by using dry-wet spinning method at different air gaps and at room temperature. The air gap was varied from 10 to 90 cm. The ultrafiltration performance of hollow fibers was studied by using aqueous solutions of polyethylene glycols and polyethylene oxides of different molecular weights. Significant difference in surface morphology between the inner and outer surface of the hollow fibers was observed by atomic force microscopy (AFM). Similar results were obtained by contact angle measurement and XPS. Mean pore sizes of the inner surface and outer surface were calculated from AFM images and compared with the pore sizes obtained from mass transport data. Pore size distribution curves were drawn from both data, i.e., from AFM images and mass-transport data, both methods gave similar results. Roughness parameters of the inner and outer surfaces and the sizes of nodular aggregates on both surfaces were measured. An attempt was made to correlate the above parameters with the performance of the membranes. Unexpected values of contact angles of both inner surface and outer surface were obtained. It was observed that the studied membranes could be put into two groups: (i) the membranes fabricated between 10 and 50 cm air gap and (ii) fabricated at higher than 50 cm air gap. A plausible mechanism for the unexpected results was discussed. J Appl Polym Sci 104: 710–721, 2007

Key words: hollow fiber; surface-modifying macromolecules; contact angle; AFM; hydrophobicity

INTRODUCTION

It is well known that the surface chemistry and morphology play an important role in the performance of ultrafiltration (UF) membrane.[1,2] The hydophobicity of the membrane surface can be increased by adding additives.[3] A less common approach to modifying the properties of a membrane surface is to introduce additives that can migrate to the film surface and alter the surface chemistry, while leaving the bulk properties intact.[4] Ward et al.[4] were apparently the first to synthesize a polyurethane block copolymer, to be used as a surface-modifying additive for the development of a new biomedical polyurethaneurea.

Surface-modifying macromolecules (SMMs) of low surface energy were used to modify the surface of UF membranes. The SMMs have an amphipathic structure consisting of a main polyurethane chain terminated with two low-polarity polymer chains. Since the surface characteristics are largely determined by the low-polarity components, they can be chosen to give a specific property. It is preferable to use a fluorine-based component because of additional features such as surface lubrication, reduced fouling, and increased chemical resistivity associated with carbon–fluorine bonds.[5,6]

The surface-modified membranes exhibited low surface energies, high chemical resistance, and good mechanical strength. Compared with the unmodified membranes, SMM modified membranes surfaces were susceptible to less fouling during UF (e.g., high fouling resistance).[5]

Khayet et al.[6] has discussed the surface modification by SMMs and its applications in membrane separation processes. These SMMs are oligomeric fluoropolymers and synthesized by polyurethane chemistry and tailored with fluorinated end groups. Several formulations for synthesis of SMMs have been developed and blended with base polymers such as polyurethanes and polyethersulfone (PES) for surface modification. In the final product, SMMs migrated to the surface, and the fluorine end groups oriented themselves toward the air–polymer interface. Thus, it increased the surface hydrophobicity. The use of SMMs has been tested for UF, pervaporation, and biomedical applications.

Correspondence to: K. C. Khulbe (khulbe@eng.uottawa.ca).

Journal of Applied Polymer Science, Vol. 104, 710–721 (2007)

Suk et al.[7] studied PES (Vicrex 4100P) modified by SMM and suggested that SMMs migrate to the surface from the cast films during evaporation. The SMMs were preferentially oriented with fluorocarbon groups at the outermost surface of the membrane, and the amount of fluorine on the surface depended on the thickness of the wet membrane. It was reported that a certain time is necessary for the migration of SMMs toward the membrane surface to occur. However, they did not study the content of fluorine in the bottom surface (cast solution/glass interface), as they prepared membranes by spreading the casting solution on a smooth glass plate and removing the solvent by evaporation at room temperature.

Pham et al.[8] developed novel SMMs for incorporation into PES membranes (flat sheet), which were intended for pervaporation applications. They reported the increase of fluorine concentration on both surfaces i.e., at the interface of casting solution/air and casting solution/glass plate. They also reported that the fluorine component at the surface was increased with increased SMM loading.

Morita et al.[9] studied the surface properties of perfluoroalkylethyl acrylate (FA)/*n*-alkyl acrylate (AA) copolymers. It was reported that the water repellency of FA/AA copolymers depended on the side chain length of AAs. The results showed that the longer the side chain length of AAs, the higher the water repellency. Water repellency was discussed from a standpoint of the molecular mobility of perfluro alkyl (RF) groups on the surface. In wet condition, more fluorine was concentrated on the polymer surface as *n* number increased, but in dry conditions, the fluorine concentration remained constant.[9,10]

In the present article, we are reporting the performance and the morphology of the surface-modified PES hollow fiber membranes fabricated by dry–wet spinning method at various air gaps. The results obtained in the present study are compared with the results obtained from the unmodified PES hollow fiber membranes.[11]

EXPERIMENTAL

Materials

PES (Ultrason E6020, MW = 58,000; flakes) and poly (vinyl pyrrolidone) (K90) were supplied by BASF Co. (Mt. Oliver, NJ) and Fluka Co. (Bucks, Switzerland), respectively. Dimethylacetamide (DMAc) (Aldrich) was used as a solvent. All other chemicals used in the experiments were of reagent grade and were used without any further purification.

Preparation of SMM

SMM was synthesized using a two-step solution polymerization under a nitrogen atmosphere. Details for the preparation of SMM are given elsewhere.[8] The reaction scheme is given in Figure 1.

Reagents used for the preparation of SMM are as follows:

i. Methylene bis-*p*-phenyl diisocyanate
ii. Polypropylene diol
iii. Zonyl BA-L intermediate
iv. *N*,*N*-Dimethylacetamide (DMAc)
v. 1,1,2-Trichloro-trifluoroethane

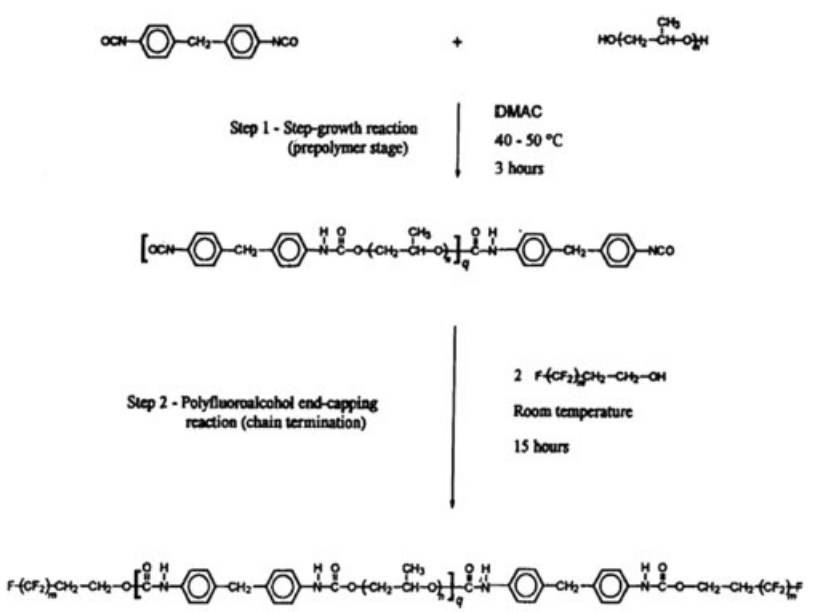

Figure 1 Reaction scheme for synthesis of surface-modifying macromolecules.

TABLE I
Conditions for the Preparation of Hollow Fibers

Casting solution	PES (18.0 wt %), PVP (3.0 wt %) and SMM (1.5 wt %) in DMAc
Temperature	Room temperature (24° C)
Air gap	10, 30, 50, 70, and 90 cm
Bore fluid rate	0.1 mL/min
Bore fluid	Distilled water
Coagulation bath	Distilled water
Spinneret pressure	2 psig
Spin rate	12 m/min

Average molecular weight of SMM was measured by gel permeation chromatography. The weight average molecular weight SMM (M_w) was 2.7×10^4, and the number average molecular weight (M_n) was 1.6×10^4.[8]

Preparation of hollow fibers

The dry–wet spinning method to prepare PEI hollow fiber membranes are described elsewhere.[12] A mixture of PES (18 wt %), PVP (3 wt %), and SMMs (1.5 wt %)[8] was used for the fabrication of the membrane. The conditions for the fabrication of hollow fibers are given in Table I. The spin rate of hollow fiber fabrication was 12 m/min.

The air gap was varied from 10 to 90 cm. After leaving the spinneret and passing through the required air gap, the hollow fibers were coagulated in a water bath at room temperature. They were immersed in an ethanol bath for 24 h. The content of the ethanol bath was replaced with fresh ethanol from time to time. After the solvent exchange, the hollow fibers were dried at room temperature. Dried fibers were used for pure water permeation experiments followed by separation measurements. The outer and inner diameters of the hollow fibers were measured by optical microscope.

AFM observation

The morphology of the surfaces of hollow fibers was studied by atomic force microscopy (AFM). Details of the tapping mode (TM)-AFM technique are given elsewhere.[11,13,14] The hollow fiber surface is characterized in terms of roughness and the size of nodule aggregates.

Pore diameters and nodule/nodular aggregate sizes on both surfaces of hollow fiber (inside and outside) were measured by visual inspection of line profiles from various AFM images of different areas of the same membrane. Figure 2 shows section analysis of TM-AFM image. To obtain the pore sizes and nodule/nodular aggregate sizes, cross-sectional line profiles were selected to traverse micron scan surface areas of the TM-AFM images. The diameters of nodules (i.e., light region or bright area, high peaks) or pores (i.e., dark area, low valleys, depression) were measured by a pair of cursors along the reference line. The horizontal distance between each pair of cursors was taken as the diameter of the nodule/nodular aggregate or pore. An example of the measurement is shown in

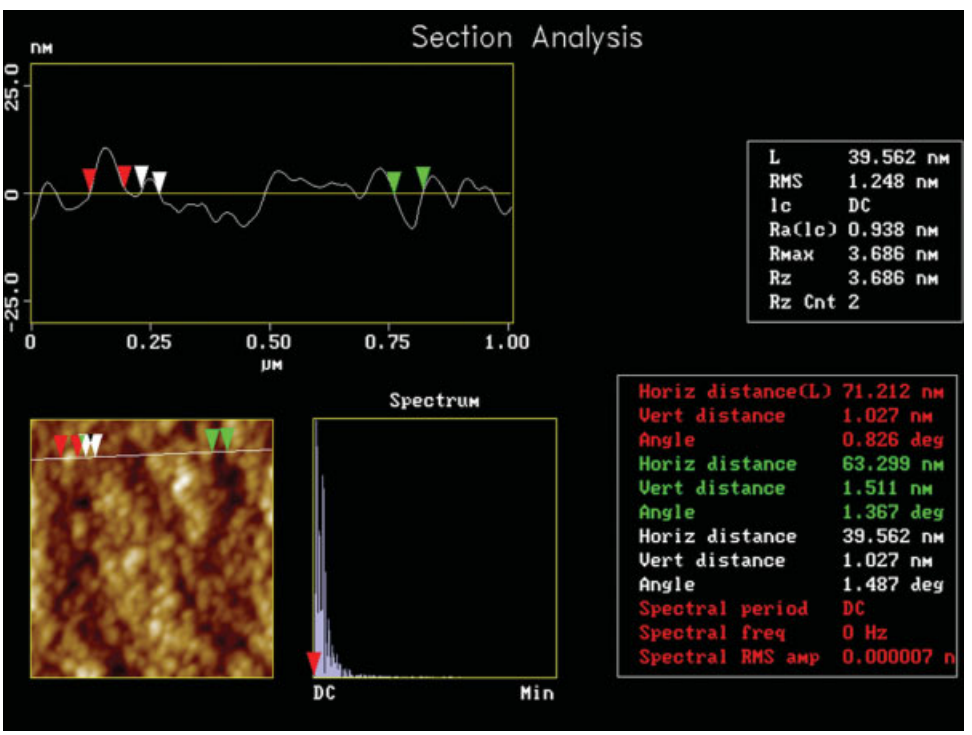

Figure 2 TM-AFM image profile. [Color figure can be viewed in the online issue, which is available at www.interscience.wiley.com.]

Figure 2. The sizes of the pores or nodule/nodular aggregates are based on the average of at least 30 measurements.

The roughness parameters obtained from AFM images should not be considered as the absolute roughness value. In the present study, the same tip was used for all experiments and all captured surfaces were treated in the same way. The evaluation of the roughness parameters of each membrane sample was based on various micron scan areas (i.e., 1×1 μm^2). Pore size distribution and porosity were calculated by the method described by Singh et al.[15]

Hollow fiber module preparation

Details of the hollow fiber module were already given earlier.[11,13] Five hollow fibers were selected and cut into a length of 15 cm and potted at both ends with epoxy glue in a test module. Around 10 cm was left for an effective length for permeation. The hollow fiber module was mounted on the test system. The test was done at room temperature and at an inside feeding pressure of 50 psig. The effective surface areas were in a range of 19.1–22.8 cm^2 based on the average of inside diameter.

Ultrafiltration experiments

The details of ultrafiltration (UF) experiments are given elsewhere.[11,13] UF experiments were conducted with aqueous feed solutions containing polyethylene glycol (PEG) (12,000; 20,000; 35,000) and polyethylene oxide (PEO) (100,000 and 200,000) of different molecular weights. The concentration of PEG and PEO was 200 ppm. A peristaltic pump supplied pure water or the feed solution to the hollow fiber module. The volume of permeates collected for a predetermined period was measured. The concentration of PEG and PEO in the feed and permeate was determined by measuring total organic carbon. The method to determine molecular weight cut-off (MWCO) and pore size distribution by UF experiments is given elsewhere.[13,15] By using pure water as feed, pure water permeation rate (PWP) was measured. After PWP measurement, separation measurements were done.

From the data obtained from pore size distribution and average pore size, the pore density of different membranes was calculated by the eq. (1).[15] After calculating the pore density, surface porosity was calculated.

$$N = \frac{128\ \eta \delta J}{\pi \Delta P \sum_{d_{\min}}^{d_{\max}} f_i d_i^4} \tag{1}$$

Where N is the total number of pores per unit area, f_1 is the fraction of the number of pores with diameter d_1, η is the solvent viscosity, and ΔP is the pressure difference across the pore, δ is the length of pores, and J is the total flux through the membrane.

The surface porosity (S_p), which is defined as the ratio between the areas of pores to the total membrane surface area was derived from eq. (2).[15]

$$S_p = \left(\frac{N\pi}{4} \sum_{d_{\min}}^{d_{\max}} f_i d_i^2 \right) \times 100 \tag{2}$$

Contact angle measurement

Contact angle measurement was carried out by goniometrically determining the angle from observation of the three-phase meniscus system at the internal and external surfaces of hollow fibers as described elsewhere in detail.[16] The goniometer (Rame Hart Model 100) was modified for hollow fiber applications.[16]

XPS study of inner and outer surfaces

The X-ray photoelectron spectroscopy (XPS) study of the surfaces of hollow fibers (inside and outside) has been done by using Kratos Axis Ultra XPS equipped with a nonmonochromated Al X-ray source. Two analyses were performed on each sample using an accelerating voltage of 14 kV and a current of 10 mA. Analysis consisted first of a survey scan performed at a pass energy of 160 eV to identify all the species present, followed by a high-resolution scans (40 eV) of the species identified by the survey scan. Peak fitting was performed using Casa XPS (ver. 2.2.99) data processing software. All analysis was calibrated to C 1s 285 eV.

RESULTS

Morphology by atomic force microscopy

Inner surface

Figures 3(a)–3(c) show the 3D AFM images of the inner surfaces of the hollow fiber membranes prepared at 10, 50, and 90 cm air gap, respectively. Similar AFM images were also observed with other studied membranes. These images are showing that there is a gradual change on the inner surface as the air gap is increasing. When comparing Figures 3(a) and 3(c), it is noticed that as the air gap is increasing, the individual nodules/nodular aggregates are separating from each other (comprising polymer aggregates known as nodules[17,18]). In Figure 3(c), the nodular aggregates are well defined. However, it was observed that nodular aggregates were not well aligned in the direction of bore fluid as observed in polyetherimide hollow fiber membranes used for UF[12,13] and in the blended PES–polyimide hollow fiber membranes used for gas separation.[14] In the polyetherimide hollow fiber membranes, there were 10–15 nodular aggregates in one row. It should be noted that the inside of the hollow fiber was in contact with water, running parallel to the spinning solution with a different speed. The shear force working on the surface of the nascent hollow

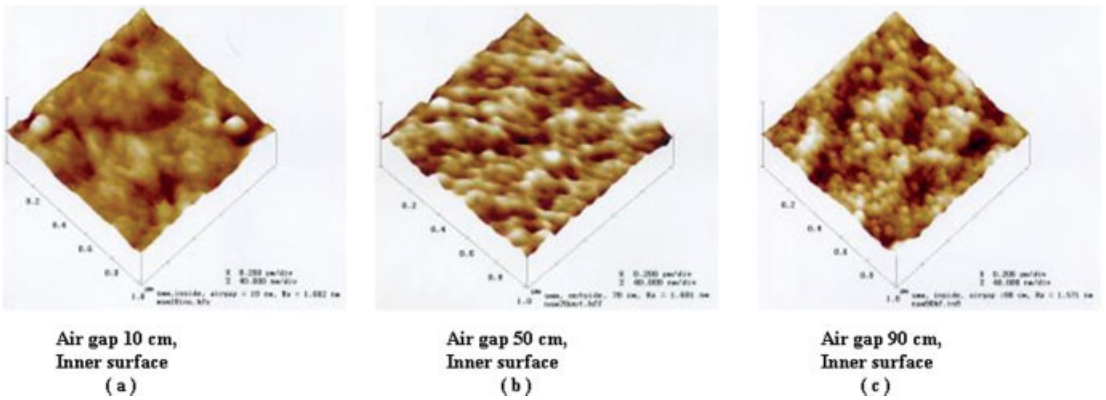

Figure 3 3D AFM images of the inner surface of hollow fiber; (a) 10 cm, (b) 50 cm, and (c) 90 cm air gap, respectively. [Color figure can be viewed in the online issue, which is available at www.interscience.wiley.com.]

fiber caused the alignment of nodular aggregates to the direction of bore fluid. This discrepancy may be due to the presence of SMM in the PES as additive. In our previous study on PES hollow fiber,[11] without SMM, it was observed that the alignment of nodular aggregates to the direction of bore fluid took place.

The average, maximum, and minimum sizes of nodular aggregates in the inner surfaces are listed in Table II. The data in Table II indicate that at 10 cm air gap, the nodules/nodular aggregate size is the smallest. It is interesting to note that the average nodular aggregate size measured on other hollow fibers (30–90 cm air gap) is almost doubled (average 65 nm).

From AFM images of inner surfaces of the studied membranes, the average pore sizes of the membranes (inner side) were calculated,[12] and the results given in Figure 4(I). Figure 4(I) indicates that after 50 cm air gap, the average pore size on the membrane surfaces increases. However, at lower air gaps (< 50 cm), the average sizes of pore are almost constant. However, no significant change is observed in roughness parameter with respect to air gap [Fig. 5(I)].

Outer surface

Figures 6(a)–6(c) show the 3D AFM images of the outer surfaces of the hollow fiber membranes prepared at 10, 50, and 90 cm air gap, respectively. Similar AFM images were also obtained with other studied membranes. From these images, it seems that the morphology of the outer surface changes gradually with a change in air gap. The nodules/nodular aggregates average sizes are given in Table II. When comparing the outer surface prepared at 10 cm air gap [Fig. 6(a)] with the inner surface [Fig. 3(a)], it seems that there is a slight difference in the morphology of the surfaces. In the outer side, the nodular aggregates are better defined.

On increasing the air gap the nodular aggregates are merging with each other and forming rougher surface. The average, maximum, and minimum size of nodular aggregates is listed in Table II. Figure 5(II) shows the roughness parameter of the outer surface versus air gap. From Figure 5(II), it seems that the roughness parameter of the studied membranes remains constant up to 50 cm air gaps. On further increasing the air gaps (between 70 and 90 cm), the roughness parameter increased markedly.

This behavior is different than that observed in polyetherimide hollow fiber membranes when fabricated in a similar way to the present study.[12] In polyetherimide hollow fiber, the roughness parameter of the outer surface decreased with an increase in air gap up to 30 cm and then leveled off.

TABLE II
Average, Maximum, and Minimum Sizes of the Nodular Aggregates on the Inner and Outer Surface of the Hollow Fibers

Air gap (cm)	Size of nodular aggregate (nm)					
	Inner surface			Outer surface		
	Average	Maximum	Minimum	Average	Maximum	Minimum
10	38.0	60.1	30.1	34.3	42.0	26.1
30	65.3	75.0	43.5	34.9	47.7	29.7
50	64.0	79.1	51.8	35.5	49.7	27.8
70	56.3	76.0	42.0	55.5	69.5	33.7
90	65.2	95.0	60.0	48.0	53.6	29.5

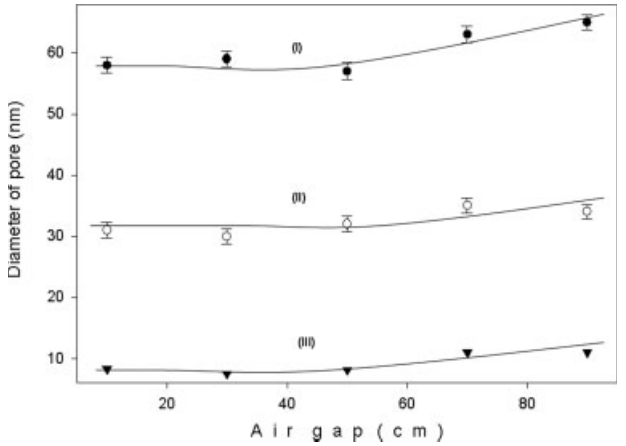

Figure 4 Diameter of pore with respect to air gap: (I) inner surface, (II) outer surface, by AFM and (III) by ultrafiltration experiments.

From AFM images of (outer surface) membranes the average pore sizes (diameter) of the outer surfaces were calculated,[12,15] and results are given in Figure 4(II). It also indicates that the average pore size on the membrane surfaces is almost constant up to 50 cm air gap. On further increasing the air gap, the average pore size also increases.

From Figure 4(II) it is clear that the average pore size in the outer surface is smaller than the inner surface. However, the average pore size in the inner and outer surfaces is in the range of 30–65 nm. Even though the pore sizes in the inner surface are larger than the outer surface, both are in the range of UF pores. Moreover, the pore size determined by the solute transport method is smaller than outer and inner surface pores [Fig. 4(III)]. Hence, from these data, it is difficult to conclude which (outer or inner) surface is controlling the membrane performance. Supplying feed solution to the inner side of the hollow fiber, therefore, does not contradict the results of the pore size measurement.

Figure 7(a) shows the mean pore size distribution on the outer surface of the membranes fabricated at 10–90 cm air gap. It can be concluded from Figure 7(a) that there are two groups of the pore size distributions, one corresponding to the air gaps of 10, 30, and 50 cm, and the other 70 and 90 cm. The mean pore sizes of the former group are smaller than the latter group.

Ultrafiltration data of the hollow fibers

Figure 8 shows the water flux with respect to air gap used to prepare the membranes. From Figure 8, it seems that flux increased very sharply up to 70 cm air gap and then decreased. The flux of the membrane prepared at 90 cm air gap is much lower when compared with that at 70 cm air gap while their average pore sizes are almost same. This is possible when the active layer corresponding to 90 cm air gap is thicker than 70 cm air gap. However, we did not measure the thickness of the active layer. Other possibilities could not be discarded such as the change in porosity etc.

Table III shows the solute separation for different molecular weights of PEG and PEO. As the molecular weight of solute is increasing, the percentage of separation is also increasing.

Pore size distribution from UF data

Figure 7(b) shows the pore size distributions of the membranes obtained by UF experiments following the method of Singh et al.[15] From Figure 7(b) it is noticed that at lower air gaps (10–50 cm air gap) the pore size distribution is sharper in comparison with at higher air gaps (70–90 cm). It seems that there are also two distinct groups. When the air gap is 10–50 cm; the mean pore size is $\sim$ 4 nm. When the air gap is 70 and 90 cm, the mean pore size is $\sim$ 8 nm. Figures 7(a) and 7(b) show a parallel relationship between pore sizes determined by two different methods.

Porosity of the membranes was calculated as described earlier and the results are given in Figure 9. Porosity of the surface is increased with the increase in air gap from10 to 50 cm. On further increasing the air gap, the porosity decreased. At higher air gap, small pores disappeared because of elongation of the nascent membrane.

Outer and inner diameter of the hollow fibers

The outer diameter (OD) and inner diameter (ID) of the hollow fibers were varied in the range from 1200 to 700 μm and 1100 to 800 μm, respectively. The decrease in OD was significant. The decrease in diameter is mainly due to elongation. Figure 10 shows thickness of

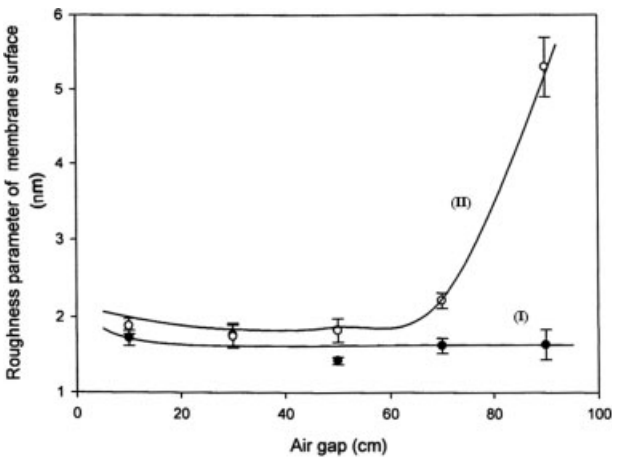

Figure 5 Roughness parameter versus air gap: (I) inner surface; (II) outer surface.

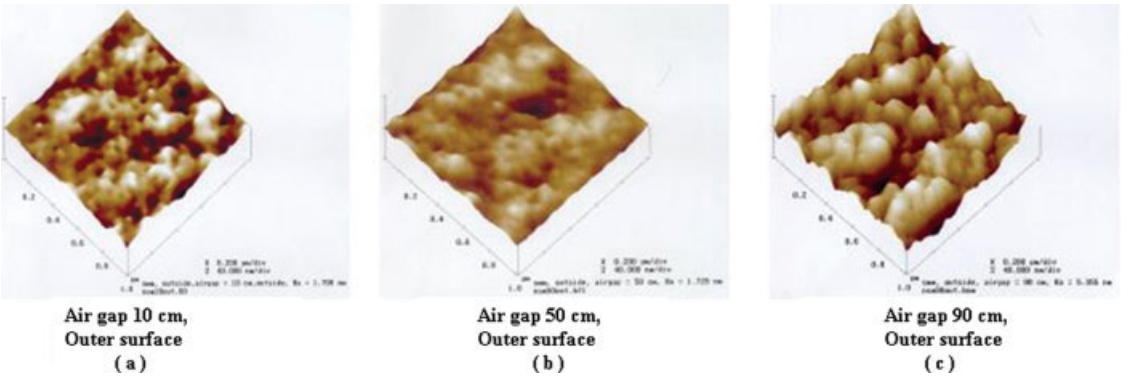

Figure 6 3D AFM images of the outer surface of hollow fiber; (a) 10 cm, (b) 50 cm, and (c) 90 cm air gap. [Color figure can be viewed in the online issue, which is available at www.interscience.wiley.com.]

the wall [(OD − ID)/2]. The figure shows that the wall thickness decreases as the air gap increases.

Contact angle of the outer and inner surface of the membrane

Figure 11 shows the contact angle of the inner surface and the outer surface versus air gap. From Figure 11, it seems that the contact angle of the inner surface is almost constant with an exception at 30 cm air gap distance where it is lower, while the contact angle of the outer surface slightly increases with the increase in air gap up to 30 cm air gap distance and then decreases significantly. The lowest contact angle was obtained for the fiber prepared at 90 cm air gap.

XPS Analysis

Figure 12 shows the XPS spectrum of the outer surface of the hollow fiber fabricated at 10 cm air gap. In this figure, no peak for fluorine was observed. It could be possible that the concentration of fluorine was very low and fluorine could not be detected under the experimental conditions. Figure 13 shows the XPS spectra for 90 cm air gap fiber. In this figure, we can detect the fluorine peak and the concentration is 1.13 atom %. Similar curves were also observed for other studied hollow fibers. The concentration of fluorine (atom %) on the surfaces with respect to air gap is given in Figure 14. The fluorine concentration also increased from 0 to 1.1 atom % at the inner surface with the increase of air gap.

DISCUSSION

It is well known that in hollow fiber spinning, the pressurized viscous solution is subjected to various stresses when it extrudes through the complicated channel within a spinneret. These stresses may influence molecular orientation and relaxation, and subsequently fiber formation and separation performance,

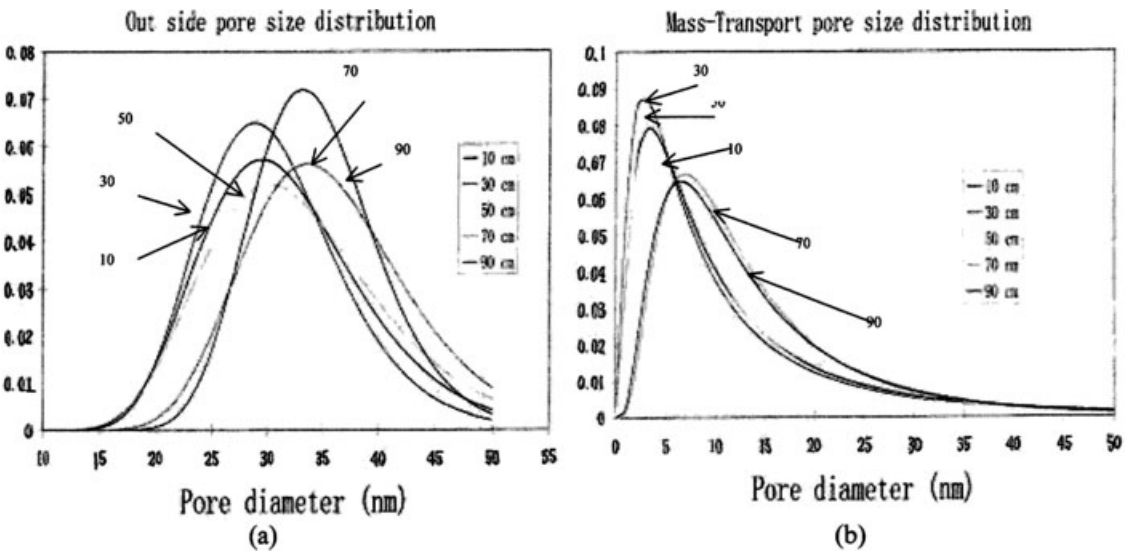

Figure 7 Pore size distribution; (a) by AFM of the outer surface, (b) by ultrafiltration experiment.

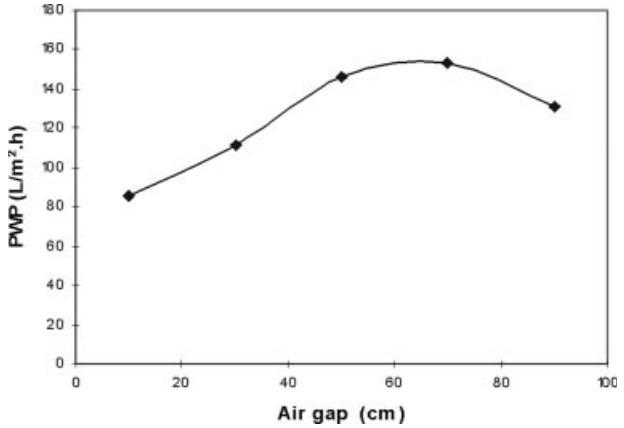

Figure 8 Water flux versus air gap.

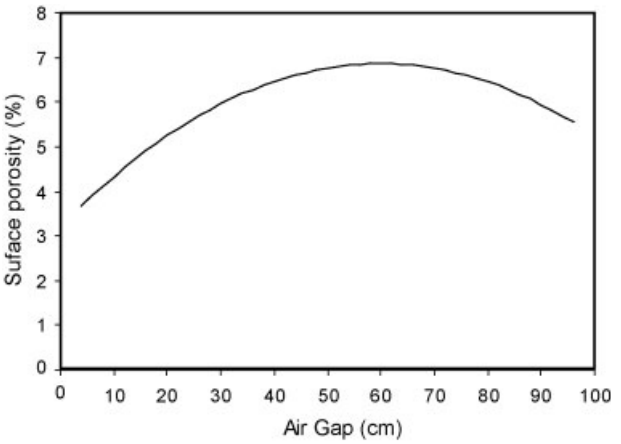

Figure 9 Porosity of membranes versus air gap.

as well as productivity.[19] Macromolecules may experience swell and relax when exiting from spinneret, if there is an air gap before coagulation and will change their orientation.

Properties of polymer, bore fluid rate, concentration of polymer, properties of solvent in the spinning solution, spinning temperature, properties of bore fluid, polymer solution flow rate, air gap, etc. all affect the performance of hollow fiber. In the present study, all the parameters were kept constant except for the air gap.

The casting solution is under stress inside the spinneret. As soon as it comes out from the spinneret, the stress perpendicular to the fiber axis will be released. The release of the stress perpendicular to the axis will result in the expansion of the fiber diameter, while stress parallel to the axis will elongate the fiber and decrease the fiber diameter. Besides this, the relaxation of polymer occurs (on outer surface) when polymer solution comes out of the spinneret.

It is found that the average pore size measured by AFM at the inner surface is around six times and at the outer surface is around three times larger than the pore size determined from the UF experiments (Fig. 4).

Similar results were obtained earlier. Khayet et al.[20] characterized the hollow fibers fabricated from polyvinylidene fluoride for UF by AFM and reported that the average pore size of the inner surface was larger than at the outer surface. They reported that the pore size of the outer surface determined by AFM was 1.8 times greater than the pore size determined by the gas permeation test and 2.7 times larger than the pore size determined by the UF test. Furthermore, Bessiéres et al. observed that AFM gave two to four times larger diameters than those obtained from the solute transport experiments.[21] According to Bessiéres et al., the pore sizes obtained from the solute transport correspond to the minimal size of the pore constriction experienced by the solute while passing through the pore, while the pore sizes measured by AFM correspond to the size of the pore entrances, which are of funnel shape and have a maximum opening at the entrance. Singh et al.[15] observed the average pore sizes of PES UF membranes measured by AFM technique were 3.5 times larger than those calculated from the solute transport data.

It is also interesting to note that the pore size increases with the air gap (Fig. 4). In particular, pore sizes seem to be split into two groups; i.e., from 10 to 50 cm air gap and from 70 to 90 cm air gap. The sudden change of the pattern above 70 cm air gap is also noticed elsewhere (Figs. 5, 7–9, 11, and 14). It is speculated that the coagulation of the inner wall was com-

TABLE III
Percentage of Separation of Different Molecular Weight PEG and PEO by SMM-PES Hollow Fiber Fabricated at Different Air Gaps

PEG and PEO (Mol. Wt. × 1000)	SMM-PES hollow fiber fabricated at different air gaps				
	10 cm (%)	30 cm (%)	50 cm (%)	70 cm (%)	90 cm (%)
8	36.28	47.32	36.85	16.78	23.68
10	48.47	63.47	65.67	51.63	47.54
12	64.88	78.65	81.03	79.62	76.25
20	73.24	85.42	87.36	85.23	81.32
35	81.96	89.67	91.02	88.65	86.58
100	90.44	90.34	91.87	91.37	88.70
200	93.25	92.16	93.64	94.63	95.5

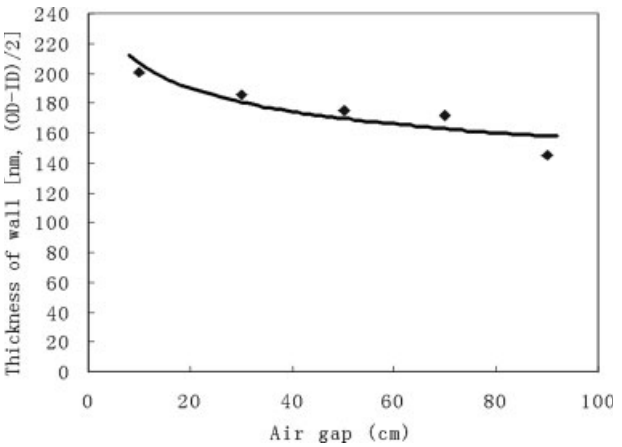

Figure 10 Thickness of the wall of the hollow fiber versus air gap.

pleted while the hollow fiber traveled the distance of 50 cm. The pattern in the morphology change may have been altered before and after the solidification of the inner wall. Other possibilities could not be discarded.

Barzin et al. span PES hollow fibers under exactly the same conditions as this work, except their hollow fibers were fabricated without blending SMM and the air gap was maintained constant at 90 cm.[11] It would be interesting to compare their data with those presented in this work. Table IV summarizes the properties of hollow fibers without[11] and with blending SMM. The analysis of AFM images indicates that roughness parameters decreased both at the inner and outer surface by blending SMM. From the UF experiments, it was found that, PWP, MWCO, and the mean pore size decreased by blending SMM. The reduction of pore size in PES/PVP membrane due to the migration of SMM toward the PES/PVP membrane surface was also observed earlier.[22]

The decrease in roughness parameter in the presence of SMM was reported earlier.[6,22] Similarly, the decrease in pore size in the presence of SMM was reported earlier.[22,23] Hamza et al. noted a significant decrease in PWP by blending SMM in their PES UF membranes.[5] Khayet observed decrease in MWCO and mean pore size calculated from UF data by blending SMM in their polyetherimide UF membranes.[24] All of the above data were for flat sheet membranes. Thus, hollow fibers exhibit exactly the same tendency in the presence of SMM.

From the XPS analysis, fluorine was found both on the inner and outer surfaces of samples except for hollow fibers spun with 10 cm air gap. Since fluorine-containing SMM was in the spinning solution, the above result is due to the limited sensitivity of XPS. In other samples, fluorine was detected as a single peak at 688.8 eV. As mentioned earlier, the fluorine content increased from 0 to about 1 atom % both at the inner and at the outer surface as the air gap increased from 10 to 90 cm. These data are interesting in three aspects. First, the fluorine concentration increases with an increase in air gap. This seems natural, since migration of SMM toward the hollow fiber surface requires a cer-

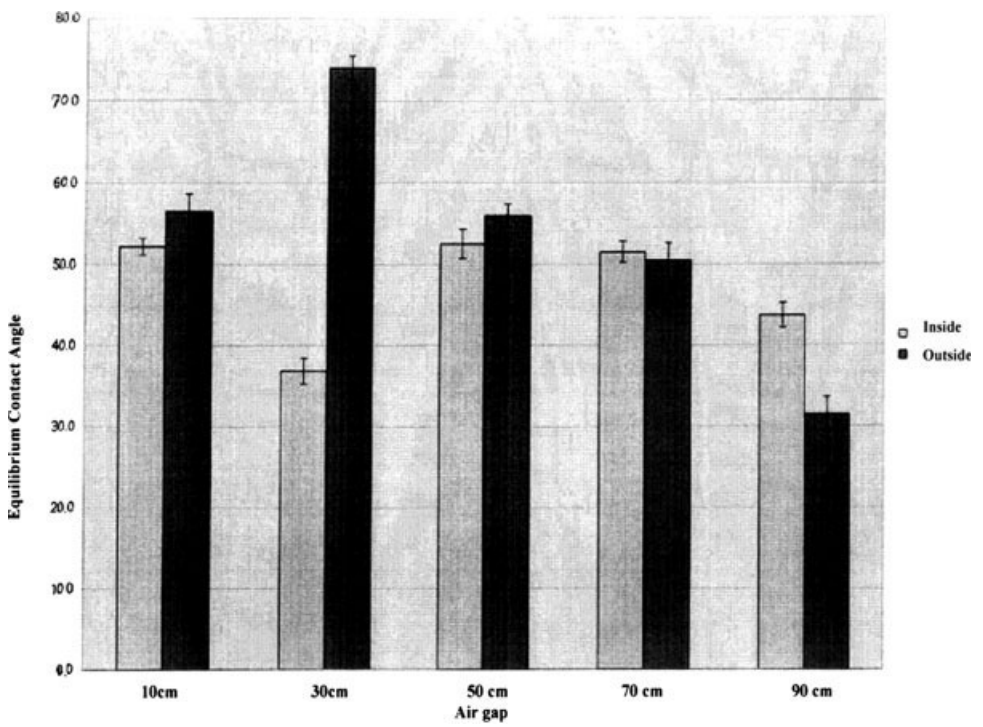

Figure 11 Contact angles of the hollow fibers, inside and outside, versus air gap.

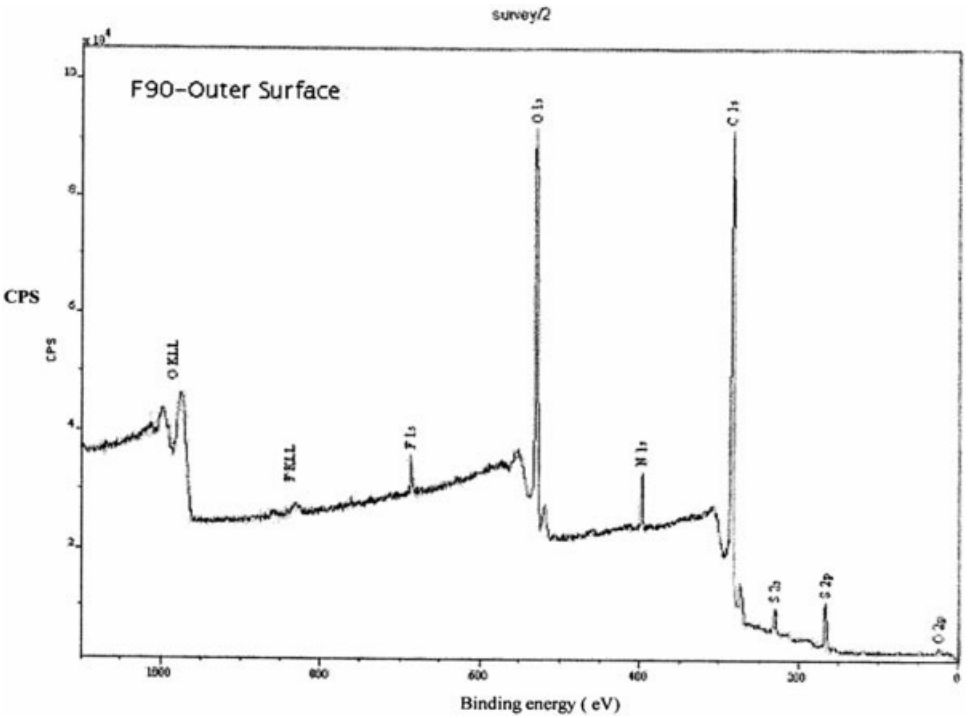

Figure 12 XPS spectrum of the outer surface of the hollow fiber fabricated at 10 cm air gap.

tain amount of time. The data on the outer surface clearly shows the increase of fluorine concentration with an increase in air gap (Fig. 14), which means an increase in the time of hollow fiber traveling in air from the spinneret to the coagulation bath. Most likely, SMM migration occurs only before the hollow fiber's entry into the coagulation bath, where the polymer structure is frozen. Second, the maximum surface fluorine content is only 1.13 atom %, which is very less when compared with 36 atom % obtained for a flat sheet membrane.[25,26] This seems also natural considering the time available for the SMMs surface migration. Although it was 8 min for the flat sheet membrane, only less than 2 s were available for the hollow fiber. Because of low fluorine concentration, a remarkable increase in surface hydrophobicity of hollow fibers cannot be expected. Third, the fluorine concentration increases on both inner and outer surface. This phe-

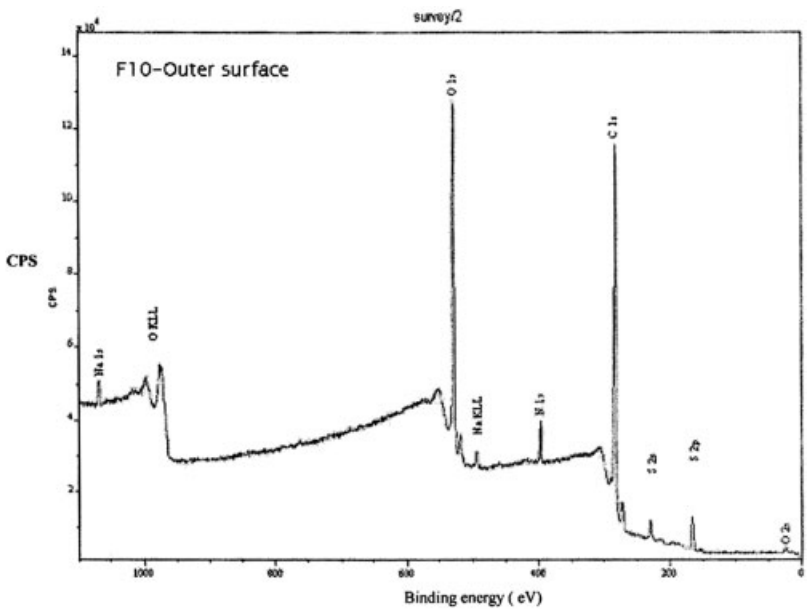

Figure 13 XPS spectrum of the outer surface of the hollow fiber fabricated at 90 cm air gap.

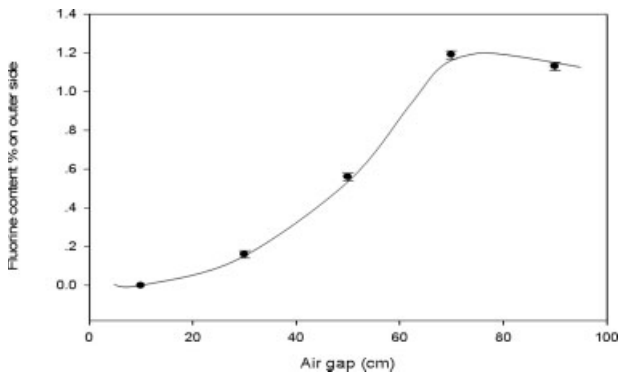

Figure 14 Fluorine concentration on the outer surface versus air gap.

nomenon is the most puzzling since the environment of the inner and outer surface is totally opposite. The polymer solution is in contact with hydrophilic water at the inner surface, while at the outer surface, polymer solution is in contact with air. This can be explained considering the amphipathic structure of SMM containing both hydrophilic polyurethane chain and hydrophobic fluorohydrocarbon end groups, and also two steps involved in the surface modification by SMM.[25,26] The first step is the SMM migration toward the surface, and the second is reorientation of fluorohydrocarbon end groups perpendicular to the surface towards air. Because of the amphipathic structure, migration will take place either towards the hydrophilic (water) or hydrophobic (air) environment. Because of the reorientation of fluorocarbon end groups, the surface fluorine content increases on both surfaces.[27] In XPS analysis of hollow fibers, the presence of sodium was detected, which might be due to contamination.

There are several reports on the contact angle of PES membranes. The contact angles increased with increasing concentration of SMMs until a plateau value was reached.[6] The presence of PVP decreased the contact angle of PES/PVP membrane, as PVP is hydrophilic.[28] The equilibrium contact angle of dense PES membrane is reported to be 67–68°.[26] The static and advancing contact angles of dense PES membrane are reported as 80° and 83–82°, respectively.[27] Ho et al.[29] reported the advancing and receding contact angles for her PES/PVP membrane as 67.2° and 26.0°, respectively. Fang,[30] on the other hand, obtained 68° and 21° for advancing and receding contact angle of the PES/PVP membrane containing 6 wt % PVP.

Equilibrium contact angles of hollow fibers were measured by the method developed by Asmanrafat.[16] The results of contact angle measurement in this work are given in Figure 11 for all hollow fiber samples spun at different air gaps and for both inner and outer surface. In Figure 11, all reported equilibrium contact angles are less than 56° except for the outer surface of the hollow fiber spun at 30 cm air gap (74°). This means all surfaces are more hydrophilic than PES material despite the presence of hydrophobic SMM, since PES equilibrium contact angle is 67–68°. From the present study, it can be concluded that the SMM migration did not affect the contact angle of the hollow fibers. This makes a sharp contrast to the effect of SMM migration on the surface of the flat sheet membranes, which brought up the advancing contact angle to the same level as that of Teflon (more than 110°).[6] The weak effect of SMM blending on the contact angle of hollow fiber surfaces is understandable considering low fluorine content, as discussed earlier.

Contact angles are used as an indicator of hydrophilicity/hydrophobicity of material. This could be true for the nonporous flat surfaces. In the hollow fiber, the surface is porous, and water enters the pores due to the capillary effect and makes the membrane surface more hydrophilic.

In the present study, the contact angle decreases with an increase in air gap on both inner and outer surfaces, except for the data for the 30 cm air gap. This seems to be the effect of the pore size on the contact angle. The pores draw water by their capillary action and make the surface more hydrophilic. The larger the pore size, the stronger becomes the effect. The contact angle decrease seems more remarkable on the outer surface. This may be due to the effect of the increased surface roughness, which is superimposed to the effect of the pore size.

It is interesting that the water flux with respect to air gap (Fig. 8) is has a similar trend to the curve obtained for fluorine concentration (Fig. 14). Increase in fluorine content should, however, enhance the hydrophobicity and decrease the water flux. Hence, Figure 8 is opposite to our expectation. The increase in PWP might be due to the pore size increase *despite* the increase in fluorine content.

It suggests that both properties, i.e., chemical (fluorine content) and morphological (pore size and roughness parameter) are influencing the membrane performance such as PWP. The effect of chemical properties is however small. Besides this, from the data obtained from AFM, UF experiments, XPS, and the measurement of the hollow fiber thickness, it can be concluded

TABLE IV
Characteristic Properties of PES/PVP (Ratio = 18/3) Hollow Fiber Membranes Prepared at 90 cm Air Gap Without and With SMM

Characterized property	Without SMM blending	With SMM blending
Roughness (nm)		
Inner surface	6.4	1.64
Outer surface	12.6	5.3
PWP (L/m^2 h)	252	131
MWCO (kDa)	200	33
Pore size by UF data (nm)	12.3	11

that these membranes can be divided into two groups, which are as follows:

1. Membranes prepared at 10–50 cm air gaps
2. Membranes prepared at 70–90 cm air gaps.

CONCLUSIONS

From the present study, following conclusions can be drawn for the effect of SMM on the hollow fiber preparation.

1. The presence of SMM in the polymer casting solution decreases the pore sizes of the hollow fiber membranes in comparison with the hollow fiber without SMM blending.
2. Fluorine content on the both surfaces, i.e., inner and outer surface increased with the increase in the air gap in the preparation of hollow fiber. This indicates the SMM migration toward both surfaces. However, compared with the flat sheet membrane with a long migration time, SMM migration was only marginal in hollow fibers.
3. AFM analysis shows that the pore sizes on the outer surface of the hollow fibers (containing SMM in polymer) have significantly smaller than on the inner surface.
4. The water flux increases with an increase in air gap, and so does the pore size. It seems that the influence of the pore size (physical property) on water flux is much stronger than the chemical effect of surface fluorine concentration.
5. In the present study, the membranes can be divided in two categories according to their AFM analysis and UF experimental results. One includes the membranes prepared at 10, 30, and 50 cm air gap and the other membranes prepared at 70 and 90 cm air gap.
6. The roughness parameter of the inner surface remains almost constant, while the roughness parameter of the outer surface increased after 50 cm air gap.
7. The contact angle is not a perfect indicator for the surface hydrophilicity of the polymer. It may depend on the surface roughness and the pore sizes. The contact angle of the outer surface was higher than the contact angle of the inner surface of the SMM blended PES hollow fibers under study.

References

1. Kesting, R. E.; Synthetic Polymeric Membranes; McGraw-Hill: New York, 1971.
2. Matsuura, T. Synthetic Membranes and Membrane Separation Processes; CRC Press: Boca Raton, FL, 1993.
3. Franken, A. C.; Nolten, J. A. M.; Mudler, M. H. V.; Bargeman, D.; Smolders, C. A. J Membr Sci 1987, 33, 315.
4. Ward, R. S.; White, K. A.; Hu, C. B. In Polyurethanes in Biomedical Engineering; Planck, H., Egbers, G., Syre, I., Eds.; Elsevier: Amsterdam, 1984.
5. Hamza, A.; Pham, V. A.; Matsuura, T.; Santerre, J. P. J Membr Sci 1997, 131, 217.
6. Khayet, M.; Suk, D. E.; Narbaitz, R. M.; Santerre, J. P.; Matsuura, T. J Appl Polym Sci 2003, 89, 2902.
7. Suk, D. E.; Chowdhury, G.; Matsuura, T.; Narbaitz, R. M.; Santerre, P.; Pleizier, G.; Deslandes, Y. Macromolecules 2002, 35, 3017.
8. Pham, V. A.; Santerre, J. P.; Matsuura, T.; Narbaitz, R. M. J Appl Polym Sci 1999, 73, 1363.
9. Morita, M.; Ogisu, H.; Kubo, M. J Appl Polym Sci 1999, 73, 1741.
10. Greenberg, S. A.; Alerey, T.; J Am Chem Soc 1954, 76, 6280.
11. Barzin, J.; Feng, C.; Khulbe, K. C.; Matsuura, T.; Madaeni, S. S.; Mirzadeh, H. J Membr Sci 2004, 237, 77.
12. Khulbe, K. C.; Feng, C. Y.; Hamad, F.; Matsuura, T.; Khayet, M. J Membr Sci 2004, 245, 191.
13. Feng, C. Y.; Khulbe, K. C.; Chowdhury, G.; Matsuura, T.; Sapkal, V. C. J Membr Sci 2001, 189, 192.
14. Khulbe, K. C.; Feng, C.; Matsuura, T.; Kapantaidakis, G. C.; Wessling, M.; Koop, G. H. J Membr Sci 2003, 226, 63.
15. Singh, S.; Khulbe, K. C.; Matsuura, T.; Ramamurthi, P. J Membr Sci 1998, 142, 111.
16. Asmanrafat, M. M.Sc. Thesis, University of Ottawa, Canada, January 2002.
17. Bridge, M. J.; Broadhead, K. W.; Hlady, V.; Tresco, P. A. J Membr Sci 2002, 195, 51.
18. Kesting, R. E. J Appl Polym Sci 1990, 41, 2739.
19. Chung, T. S.; Qin, J. J.; Gu, J. Chem Eng Sci 2000, 55, 1077.
20. Khayet, M.; Feng, C. Y.; Khulbe, K. C.; Matsuura, T. Polymer 2002, 43, 3879.
21. Bessières, A.; Meireles, M.; Coratger, R.; Beauvilliain, J.; Sanchez, V. J Membr Sci 1996, 109, 271.
22. Mosqueda-Jimenez, D. B.; Narbaitz, R. M.; Matsuura, T. Sep Purif Tech 2004, 37, 51.
23. Zhang, L.; Chowdhury, G.; Feng, C.; Matsuura, T.; Narbaitz, R. J Appl Polym Sci 2003, 88, 3132.
24. Khayet, M.; Feng, C. Y.; Matsuura, T. J Membr Sci 2003, 213, 159.
25. Suk, D. E. Ph.D. Thesis, University of Ottawa, Canada, 2006.
26. Suk, D. E.; Pleizer, G.; Deslandes, Y.; Matsuura, T. Desalination, 2002, 149, 303.
27. Kaplan, M. C.; Jégou, A.; Chaufer, B.; Rabiller-Bandry, M.; Michalsky, M. C. Desalination, 2002, 146, 149.
28. Miyano, T.; Matsuura, T.; Carlsson, D. J.; Sourirajann, S. J Appl Polym Sci 1990, 41, 407.
29. Ho, J. Y.; Matsuura, T.; Santerre, J. P. J Biomater Sci Polym Ed 2000, 11, 1085.
30. Fang, Y. Ph.D. Thesis, University of Ottawa, Ottawa, Canada, 1997.